2-2015

Modeling inward diffusion and slow decay of energetic electrons in the Earth's outer radiation belt

Q. Ma
University of California - Los Angeles

W. Li
University of California - Los Angeles

R. M. Thorne
University of California - Los Angeles

B. Ni
Wuhan University of Science and Technology

C A. Kletzing
University of Iowa

See next page for additional authors

Recommended Citation
Q. Ma, W. Li, R. M. Thorne, B. Ni, C. A. Kletzing, W. S. Kurth, G. B. Hospodarsky, G. D. Reeves, M. G. Henderson, H. E. Spence, D. N. Baker, J. B. Blake, J. F. Fennell, S. G. Claudepierre, and V. Angelopoulos, 'Modeling inward diffusion and slow decay of energetic electrons in the Earth's outer radiation belt', Geophysical Research Letters, vol. 42, no. 4, pp. 987–995, Feb. 2015.

AGU PUBLICATIONS

Geophysical Research Letters

RESEARCH LETTER
10.1002/2014GL062977

Key Points:
- We simulated the observed gradual diffusion processes of energetic electrons
- Radial diffusion processes caused the observed intrusion of energetic electrons
- Hiss and EMIC waves caused the observed energetic electron decay in 10 days

Supporting Information:
- Text S1
- Readme
- Figure S1
- Figure S2

Correspondence to:
Q. Ma,
qianlima@atmos.ucla.edu

Citation:
Ma, Q., et al. (2015), Modeling inward diffusion and slow decay of energetic electrons in the Earth's outer radiation belt, *Geophys. Res. Lett.*, *42*, 987–995, doi:10.1002/2014GL062977.

Received 23 DEC 2014
Accepted 30 JAN 2015
Accepted article online 3 FEB 2015
Published online 25 FEB 2015

Modeling inward diffusion and slow decay of energetic electrons in the Earth's outer radiation belt

Q. Ma[1], W. Li[1], R. M. Thorne[1], B. Ni[2], C. A. Kletzing[3], W. S. Kurth[3], G. B. Hospodarsky[3], G. D. Reeves[4], M. G. Henderson[4], H. E. Spence[5], D. N. Baker[6], J. B. Blake[7], J. F. Fennell[7], S. G. Claudepierre[7], and V. Angelopoulos[8,9]

[1]Department of Atmospheric and Oceanic Sciences, University of California, Los Angeles, Los Angeles, California, USA, [2]Department of Space Physics, School of Electronic Information, Wuhan University, Wuhan, China, [3]Department of Physics and Astronomy, University of Iowa, Iowa City, Iowa, USA, [4]Space Science and Applications Group, Los Alamos National Laboratory, Los Alamos, New Mexico, USA, [5]Institute for the Study of Earth, Oceans, and Space, University of New Hampshire, Durham, New Hampshire, USA, [6]Laboratory for Atmospheric and Space Physics, University of Colorado, Boulder, Colorado, USA, [7]The Aerospace Corporation, Los Angeles, California, USA, [8]Department of Earth, Planetary, and Space Sciences, University of California, Los Angeles, Los Angeles, California, USA, [9]Institute of Geophysics and Planetary Physics, University of California, Los Angeles, Los Angeles, California, USA

Abstract A new 3-D diffusion code is used to investigate the inward intrusion and slow decay of energetic radiation belt electrons (>0.5 MeV) observed by the Van Allen Probes during a 10 day quiet period on March 2013. During the inward transport, the peak differential electron fluxes decreased by approximately an order of magnitude at various energies. Our 3-D radiation belt simulation including radial diffusion and pitch angle and energy diffusion by plasmaspheric hiss and electromagnetic ion cyclotron (EMIC) waves reproduces the essential features of the observed electron flux evolution. The decay time scales and the pitch angle distributions in our simulation are consistent with the Van Allen Probe observations over multiple energy channels. Our study suggests that the quiet time energetic electron dynamics are effectively controlled by inward radial diffusion and pitch angle scattering due to a combination of plasmaspheric hiss and EMIC waves in the Earth's radiation belts.

1. Introduction

The Earth's outer electron radiation belt is highly variable due to various source and loss processes [e.g., *Reeves et al.*, 2003; *Thorne*, 2010; *Turner et al.*, 2014]. The dynamics of energetic electrons in the Earth's outer radiation belt is strongly affected by wave-particle interactions, and the evolution of the electron population can be reasonably described using quasi-linear theory [*Kennel and Engelmann*, 1966; *Lyons*, 1974a, 1974b]. Electrons resonant with ultralow frequency (ULF) waves violate the third adiabatic invariant and undergo radial diffusion, causing radial electron transport [e.g., *Cornwall*, 1972; *Shprits et al.*, 2008a; *Ozeke et al.*, 2014]. Electrons resonant with higher-frequency electromagnetic waves violate the first and second adiabatic invariants and undergo pitch angle and energy diffusion, causing precipitation losses into the atmosphere and energy exchange with the waves [e.g., *Albert and Young*, 2005; *Glauert and Horne*, 2005; *Shprits et al.*, 2008b; *Xiao et al.*, 2009, 2010].

During quiet geomagnetic periods, the evolution of the energetic electron population in the Earth's outer radiation belt is governed by the source caused by radial diffusion and the loss due to pitch angle scattering [e.g., *Schulz and Lanzerotti*, 1974]. The equilibrium structure of the Earth's radiation belt below ~1 MeV has been modeled as a balance between radial diffusion and pitch angle scattering loss due to whistler mode waves [*Lyons and Thorne*, 1973]. Recent radiation belt modeling has shown that plasmaspheric hiss is a major candidate for the loss of energetic electrons at energies higher than tens of keV inside the plasmasphere [e.g., *Thorne et al.*, 2013; *Ni et al.*, 2013, 2014] and that electromagnetic ion cyclotron (EMIC) waves can cause efficient losses of highly relativistic (>MeV) electrons [e.g., *Horne and Thorne*, 1998; *Li et al.*, 2007; *Kersten et al.*, 2014].

The gradual diffusion of energetic electrons in the 10 day period in March 2013 provides a unique opportunity for a quantitative study of quiet time electron evolution [*Baker et al.*, 2014]. During the ~10 day period prior to

the 17 March 2013 geomagnetic storm, the Van Allen Probes observed the gradual inward transport and weak loss of relativistic electron fluxes in the energy channels up to ~10 MeV. Coupling of real-time radial diffusive transport and pitch angle scattering loss is required to explain the detailed electron flux evolution. In this paper we use a three-dimensional radiation belt model to reconstruct the evolution of electron fluxes in multiple energy channels and quantitatively evaluate the roles of radial diffusion and pitch angle scattering due to both plasmaspheric hiss and EMIC waves.

2. Observations of Electrons and Waves in March 2013

The Van Allen Probes are equipped with high-quality scientific instruments to provide reliable particle and field measurements in the Earth's inner magnetosphere [*Mauk et al.*, 2012]. The Energetic Particle Composition and Thermal Plasma (ECT) suite [*Spence et al.*, 2013] measures the radiation belt particle spectra with excellent energy and pitch angle resolution. The Magnetic Electron Ion Spectrometer (MagEIS) instrument [*Blake et al.*, 2013] measures the energetic electrons over the energy range of ~30 keV to ~4 MeV, and the Relativistic Electron Proton Telescope (REPT) instrument [*Baker et al.*, 2012] measures the highly energetic electrons from ~1.5 MeV to ~20 MeV. The Electric and Magnetic Field Instrument Suite and Integrated Science (EMFISIS) [*Kletzing et al.*, 2013] measures the DC magnetic field (magnetometer) and the wave electric and magnetic fields (Waves instrument). The waveform receiver of the Waves instrument measures wave spectra from 10 Hz to 12 kHz for both electric and magnetic fields. In addition, the search coil magnetometer [*Roux et al.*, 2008] on board the Time History of Events and Macroscale Interaction during Substorms (THEMIS) spacecraft [*Angelopoulos*, 2008] provides magnetic fluctuation measurements up to ~4 kHz. During March 2013, the Van Allen Probes sampled the outer radiation zone around the midnight sector, and the THEMIS spacecraft made observations near noon and on the dawnside; wave measurements from both missions are used to obtain the global distribution of the waves.

Figure 1 presents an overview of the energetic electron flux evolution from 1 to 21 March 2013. Figures 1a–1c show the B_z component of the interplanetary magnetic field (IMF), the solar wind dynamic pressure, and the *Dst* index, respectively. On 1 March, the solar wind pressure gradually increased to ~8 nPa, leading to a modest storm with a minimum *Dst* index ~ −50 nT. After the recovery phase of the first storm, the geomagnetic condition remained relatively quiet for ~10 days until the arrival of a strong interplanetary shock on 17 March [*Baker et al.*, 2014; *Li et al.*, 2014], when the IMF B_z turned strongly southward, the solar wind pressure rapidly increased to above 20 nPa, and the *Dst* index dropped to below −100 nT. During the relatively quiet 10 day interval (shaded area), the plasmapause location remained mostly outside ~5 R_E, and the THEMIS spacecraft observed weak chorus waves on the dayside outside the plasmapause (Figure 1d). The plasmapause location was estimated from the upper hybrid line (not shown) measured on the EMFISIS Waves instrument when the satellite crossed the upper hybrid resonance frequency with a density of 50 cm^{-3}. Moderately strong plasmaspheric hiss in the frequency range of 80–4000 Hz, which may cause the decay of energetic electrons, was observed by the THEMIS spacecraft near noon during the inbound path (Figure 1e). The Van Allen Probes observed weaker plasmaspheric hiss waves on the nightside (Figure 1f), providing additional information on the global hiss wave distributions. Figure 1g shows the electron flux for an energy of 80.4 keV and a pitch angle of 90° as a function of L^*, calculated based on the TS05 magnetic field model [*Tsyganenko and Sitnov*, 2005]. Strong injections of plasma sheet electrons were observed during the geomagnetic storms on 1 and 17 March, respectively. During the 10 day quiet period, only weak variations in the plasma sheet electron flux were observed near $L^* = 5.5$, consistent with the weak chorus activity in Figure 1d. The highly relativistic electron flux (at 3.60 MeV) exhibits a clear tendency for gradual inward radial diffusion (Figure 1h). At 12:00 UT on 6 March, the peak of the electron flux for an energy of 3.6 MeV was at around $L^* = 4.5$. The peak of the electron flux gradually moved inward to $L^* = 4.0$ and slowly decayed by approximately an order of magnitude over 10 days. The radial diffusion features can be more clearly identified from the electron flux measurements at a constant energy than the phase space density measurements at a constant μ [*Baker et al.*, 2014]. The observations of the waves and energetic electrons during the quiet period suggest that the electron evolution is caused by the simultaneous processes of radial diffusion and slow scattering loss inside the Earth's plasmasphere.

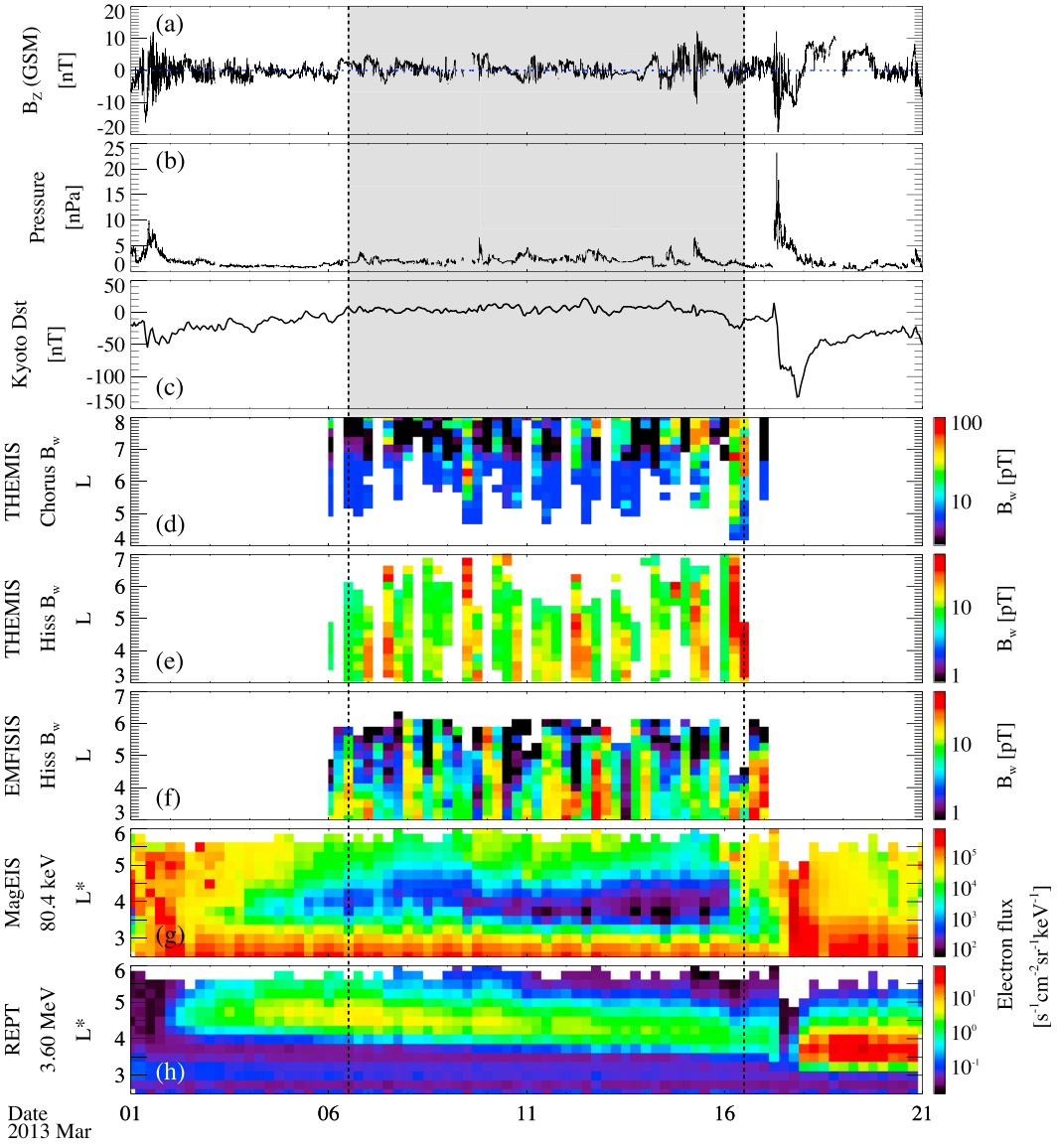

Figure 1. Evolution of waves and electrons observed by Van Allen Probes and THEMIS during 1–21 March 2013. (a) The near-Earth solar wind B_z in the GSM coordinate, (b) solar wind dynamic pressure, (c) *Dst* index, (d) THEMIS observations of chorus magnetic wave amplitude (B_w), (e) hiss B_w, (f) Van Allen Probe observation of hiss B_w, (g) electron differential flux for a pitch angle of ~90° and an energy of ~80.4 keV, and (h) electron differential flux for a pitch angle of ~90° and an energy of ~3.60 MeV. The area between the two vertical black dashed lines indicates the simulation interval.

3. Simulation of the Gradual Diffusion Processes

Radial diffusion of electrons can be caused by interaction with ULF waves, which are associated with electric and magnetic fluctuations in the magnetosphere. *Brautigam and Albert* [2000] used the Combined Release and Radiation Effects Satellite data to obtain the electric component (D_{LL}^E) and magnetic component (D_{LL}^M) of the radial diffusion coefficient (D_{LL}) as a function of *Kp*, *L* shell, and electron energy (see supporting information). The time scale of radial diffusion for ~1 MeV equatorially mirroring electrons at *L*~5 when *Kp*~2 is about 14 days. Therefore, radial diffusion is likely a reasonable cause of the observed inward intrusion of energetic electrons during the 10 day period.

Plasmaspheric hiss and EMIC waves can both be effective for scattering energetic electrons near the loss cone. Hiss and EMIC waves are known to occur in selective magnetic local time (MLT) regions [*Meredith et al.*, 2013, 2014], which may not be sampled by an individual spacecraft. Consequently, to construct a realistic

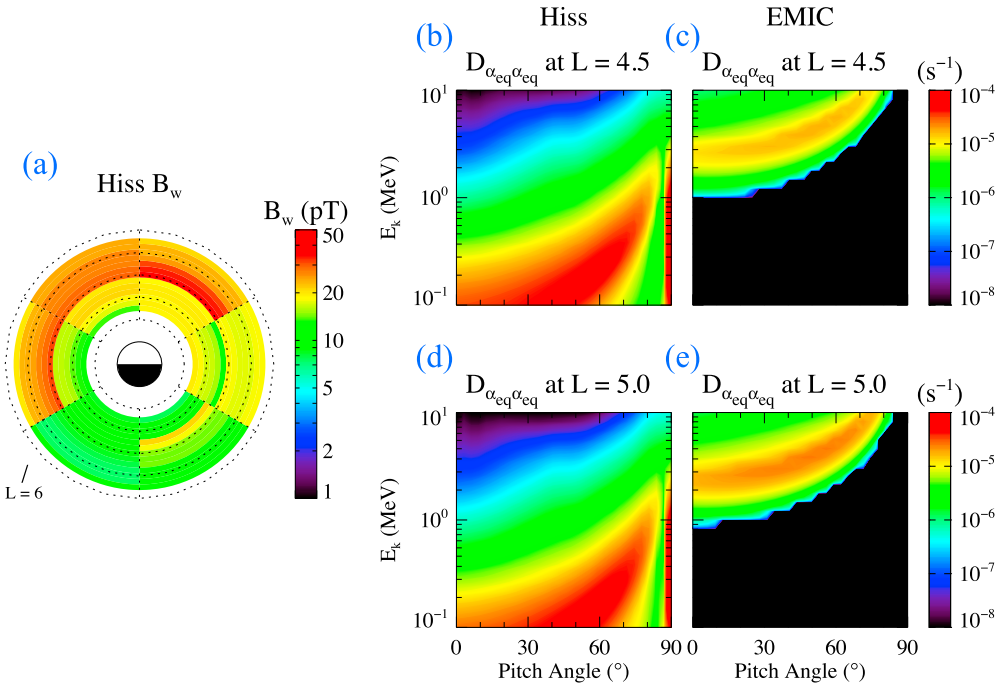

Figure 2. Averaged magnetic wave amplitudes on a global scale and electron pitch angle diffusion coefficients. (a) The global distribution of hiss B_w averaged over the 10 day period constructed based on in situ spacecraft observations combined with quiet time statistical results. (b) Bounce- and drift-averaged pitch angle diffusion coefficients of plasmaspheric hiss as a function of pitch angle and energy obtained using the 10 day root-mean-square averaged B_w at $L = 4.5$. (c) Bounce- and drift-averaged pitch angle diffusion coefficients ($D_{\alpha eq \alpha eq}$) of EMIC waves at $L = 4.5$ during the periods when $Kp \geq 2$, with an MLT coverage of 25% and an occurrence rate of 2%. (d) The same as in Figure 2b but for $L = 5.0$. (e) The same as in Figure 2c but for $L = 5.0$.

global hiss wave model, we first identified the hiss magnetic wave amplitude B_w observed by all three Earth-orbiting THEMIS spacecraft near noon and dawnside (Figure 1e) and Van Allen Probes (Figure 1f) on the nightside every 6 h to obtain the real-time distribution of the root-mean-square plasmaspheric hiss wave amplitudes. To obtain the full global distribution of hiss B_w data, the entire 1.5 years of Van Allen Probes B_w survey (not shown) is used to calculate the B_w ratios in different MLT regions during quiet periods. B_w values at regions not sampled by the spacecraft during the period under study are then calculated using the combination of the statistical B_w ratios and the localized observation of hiss B_w data from Van Allen Probes and THEMIS. The global distribution of hiss B_w data averaged over the 10 day period is shown in Figure 2a. Hiss wave amplitudes are strongest on the dayside and between $L = 4$ and 5, and the wave amplitude averaged over all MLTs and between $L = 4$ and 5 is ~18 pT, which is roughly consistent with the statistical survey during quiet to modest time periods by *Meredith et al.* [2004].

Drift- and bounce-averaged diffusion coefficients are calculated using the University of California, Los Angeles (UCLA) full diffusion code [*Ni et al.*, 2008, 2011; *Shprits and Ni*, 2009] by including the harmonic resonances from −10 to +10, which is shown to be adequate to account for the accurate values of pitch angle diffusion rates for plasmaspheric hiss (see supporting information). The hiss wave frequency spectra from ~20 Hz to ~4 kHz at different MLT sectors and L shells were obtained from the 1.5 years of Van Allen Probe survey of the hiss waves during quiet periods (see Figure S2 in the supporting information for hiss wave spectrum near noon at $L = 4.5$). Between $L = 4.5$ and 5, the statistical peak hiss wave frequencies lie between 100 and 200 Hz for different MLT sectors. A latitudinally varying wave normal angle distribution of plasmaspheric hiss from *Ni et al.* [2013] is used in the calculation, which is roughly consistent with the Cluster statistics by *Agapitov et al.* [2013]. The total plasma density is obtained from the empirical plasmaspheric density model by *Sheeley et al.* [2001]. The resultant pitch angle diffusion coefficients at $L = 4.5$ and $L = 5.0$ averaged over the 10 day period are shown in Figures 2b and 2d, respectively, which are representative for diffusion coefficients over $L \geq 4$. The hiss wave pitch angle diffusion coefficients near the loss cone decrease

with ~$(p^{3/2}\gamma)^{-1}$, where p is the momentum and γ is the Lorentz factor, as expected by *Ripoll et al.* [2014]. At energies below ~1 MeV, plasmaspheric hiss can cause pitch angle scattering into the loss cone over a time scale of tens of days, consistent with the observation by the MagEIS instrument. However, the scattering is much weaker at higher energies, indicating the need for an additional loss process for the highly relativistic electron population (>1 MeV).

EMIC waves can be effective for the loss of multiple MeV electrons in the Earth's inner magnetosphere [*Li et al.*, 2007; *Thorne*, 2010; *Sakaguchi et al.*, 2013; *Usanova et al.*, 2014; *Kersten et al.*, 2014]. However, direct EMIC wave observations in the region $<6\ R_E$ were very limited over the 10 day period. Van Allen Probes observed two EMIC wave events, each lasting tens of minutes on the nightside, and THEMIS observed two EMIC wave events, each lasting tens of minutes on the dayside. Consequently, to model the effect of EMIC waves, we assumed that when $Kp \geq 2$, the helium band EMIC waves with a modest intensity of $B_w^2 = 0.1\ \mathrm{nT}^2$ are present at $L \geq 4$ over 25% of MLTs with an occurrence rate of 2%, consistent with the recent statistical study by *Meredith et al.* [2014]. We calculate the diffusion rates of the helium band EMIC wave with a central frequency, frequency bandwidth, and lower and upper cutoff frequencies of 3.6 f_{O+}, 0.25 f_{O+}, 3.35 f_{O+}, and 3.85 f_{O+}, respectively, where f_{O+} is the oxygen gyrofrequency. The wave normal is assumed to be field aligned, and the waves have a maximum latitudinal distribution of 45°. A multispecies magnetospheric plasma is assumed composed of 70% H^+, 20% He^+, and 10% O^+, following *Meredith et al.* [2003] and *Lee and Angelopoulos* [2014]. The drift- and bounce-averaged pitch angle diffusion coefficients of the EMIC waves at $L = 4.5$ and $L = 5.0$, when $Kp \geq 2$, are shown in Figures 2c and 2e, respectively, which are representative for diffusion coefficients over $L \geq 4$. Although the adopted EMIC waves cannot scatter electrons with energy lower than ~1 MeV, they can effectively cause the loss of multiple MeV electrons within about 10 days, roughly consistent with the REPT observation. The EMIC wave scattering effects depend on the wave frequency spectrum, and the adopted weak helium band EMIC waves with a central frequency of ~3.6 f_{O+} primarily influence the energetic electron populations with energies higher than 1 MeV.

We have recently developed a new three-dimensional radiation belt model to simulate the energetic electron flux evolution between $L = 2.5$ and $L = 5.5$ from 12:00 UT on 6 March 2013 to 12:00 UT on 16 March 2013, as described in the supporting information. The energy ranges increase with decreasing L shell and are set as from 0.18 MeV to 5.8 MeV at $L = 5.5$ and from 1.1 MeV to 20 MeV at $L = 2.5$. The phase space densities (PSDs) at the higher L shell boundary and lower-energy boundary are obtained from the Van Allen Probe measurements. We assume the absence of particles at the lower L shell boundary and higher-energy boundary. For equatorial pitch angles inside the loss cone, we set the PSD to be zero to simulate an empty loss cone. At the higher pitch angle boundary, we use a zero gradient condition to simulate the flat pitch angle distribution at 90°.

Our simulation of electron flux evolution in multiple energy channels in comparison with observation is shown in Figure 3. The measurements by the MagEIS instrument (Figures 3a and 3b) and the REPT instrument (Figures 3c and 3d) clearly show the gradual inward diffusion and slow decay of the 0.59–3.60 MeV electrons. Figure 3e shows the 10 day variations of Kp index multiplied by 10 (black), hiss wave B_w averaged between $L = 4$ and $L = 5$ and all MLT sectors (red), and EMIC wave B_w divided by 10 (blue). The simulated evolution of 0.59–3.60 MeV electron fluxes with a pitch angle of 90° is shown in Figures 3f–3i, respectively, which agrees fairly well with the Van Allen Probe observations in Figures 3a–3d. During the 10 day period, both the observations and our simulation results show that (1) the peak location of 2 MeV and 3.6 MeV electron fluxes gradually moved inward by ~0.5 R_E and the radial intrusion rate is correlated with the Kp variations, and (2) the peak values of the electron fluxes gradually decreased by about an order of magnitude and the decay rates are correlated with the wave intensity variations. For example, at around 18:00 UT on 12 March, as the hiss and EMIC B_w increase, the electron fluxes from 0.59 MeV to 3.60 MeV clearly decay; at around 06:00 UT on 15 March, as Kp index increases, the peak of the electron flux moves to lower L shells. In Figure 3j, we simulated the electron flux evolution without including EMIC wave scattering to test the role of the EMIC waves. The pitch angle scattering rates of ~3.6 MeV electrons by plasmaspheric hiss waves are ~$10^{-7}\ \mathrm{s}^{-1}$, and therefore, hiss waves alone cannot cause the clear decaying feature within 10 days. The inward radial intrusion of the energetic electrons in Figure 3j is similar to the simulation result including EMIC waves (Figure 3i), but instead of decaying, the electron flux increases in association with the inward radial transport. Note that without loss to the atmosphere, the 3.60 MeV equatorially mirroring electrons at around $L = 4$ at

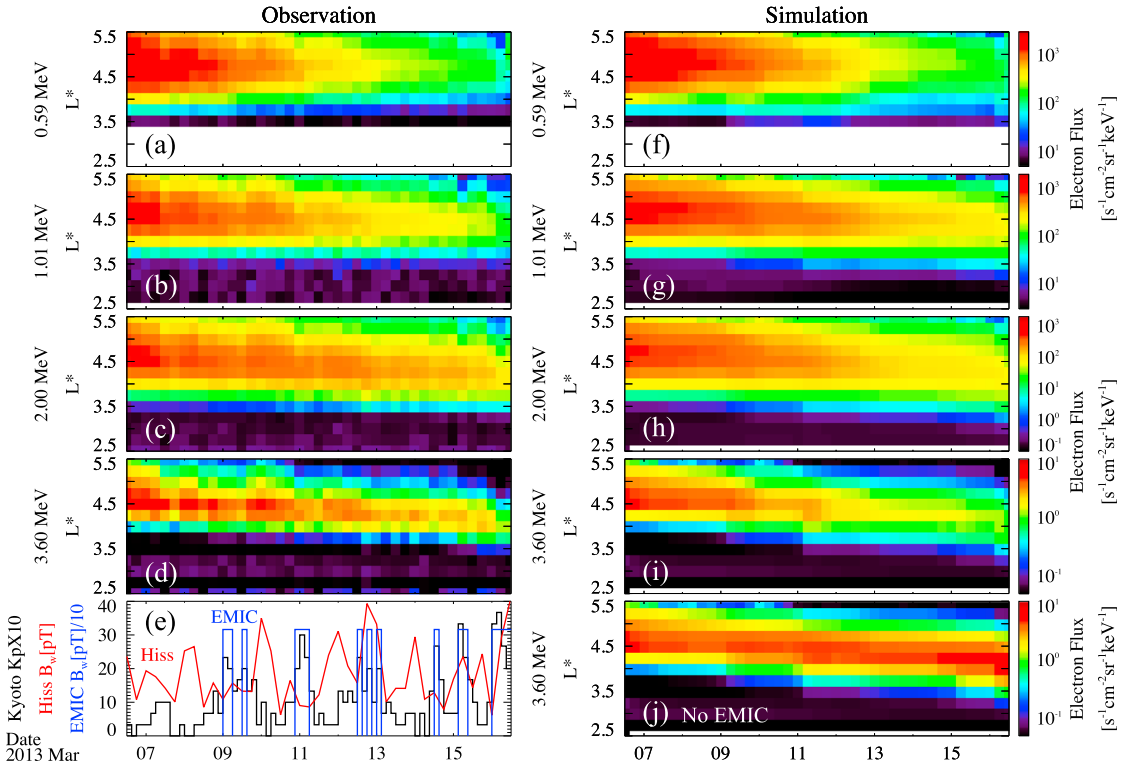

Figure 3. The comparison between the observation and simulation of equatorially mirroring electron fluxes from 12:00 UT on 6 March to 12:00 UT on 16 March 2013. The Van Allen Probe observation of electron differential flux as a function of L^* for an energy of (a) 0.59 MeV, (b) 1.01 MeV, (c) 2.00 MeV, (d) 3.60 MeV, and (e) the Kyoto *Kp* index multiplied by 10 (black line), the hiss wave amplitude averaged over $L = 4$ to 5 (red line), and the EMIC wave amplitude with an intensity of $B_w^2 = 0.1\ \mathrm{nT}^2$ when $Kp \geq 2$ (blue line). Full simulation results of electron differential flux as a function of L^* for an energy of (f) 0.59 MeV, (g) 1.01 MeV, (h) 2.00 MeV, (i) 3.60 MeV, and simulation of the electron differential flux evolution without EMIC wave scattering for an energy of (j) 3.60 MeV.

12:00 UT on March 16 simply originate from the ~2.95 MeV (with much higher fluxes) equatorially mirroring electrons at around $L = 4.5$ at 12:00 UT on March 6. Although the EMIC waves in our simulation are weak ($B_w^2 = 0.1\ \mathrm{nT}^2$) and occurrence rates are low (2% for the period when $Kp \geq 2$), they can contribute to reduce electron fluxes at >~1 MeV within 10 days, which is consistent with the observed electron dynamics.

Radial diffusion, pitch angle scattering by hiss waves, and pitch angle scattering by EMIC waves can individually cause different evolutions of the electron pitch angle distributions. Figure 4 presents the pitch angle distribution profiles of the 0.59–3.6 MeV electron fluxes at L~4.5 from observations and different simulation results. The simulations including radial diffusion and local scattering by hiss and EMIC waves (referred to as "full simulation"; the black solid lines in Figure 4) provide the best agreement with the observations (diamond symbols in Figure 4) at multiple energy channels, quantitatively reproducing the evolution of the pitch angle distribution profiles as well. Hiss wave scattering causes flattened pitch angle distribution profiles over a wide range of pitch angles, as shown in the full simulation results and the observational data. The simulation without hiss wave scattering (red dashed lines in Figure 4) overestimates the electron fluxes with energies lower than ~1 MeV due to the lack of significant loss processes; at higher energies, the EMIC waves cause the rapid loss of electrons with pitch angles lower than ~60–70° but cannot interact with the electrons with higher pitch angles. The simulation without EMIC wave scattering (green dashed lines in Figure 4) provides the same profiles with the full simulation for energies lower than ~1 MeV but overestimates the electron fluxes at higher energies. The purely radial diffusion process (blue solid lines in Figure 4) causes an energization of the electrons when they diffuse inward and overestimates the energetic electron fluxes. The purely local diffusion simulation (cyan solid lines in Figure 4) reproduces the decay rates and pitch angle distribution profiles but cannot explain the inward intrusion of the energetic electrons. Overall, Figure 4 clearly shows that the pitch angle scattering loss of electrons at lower and higher energies is effectively caused by the hiss waves and EMIC waves, respectively, and the hiss wave

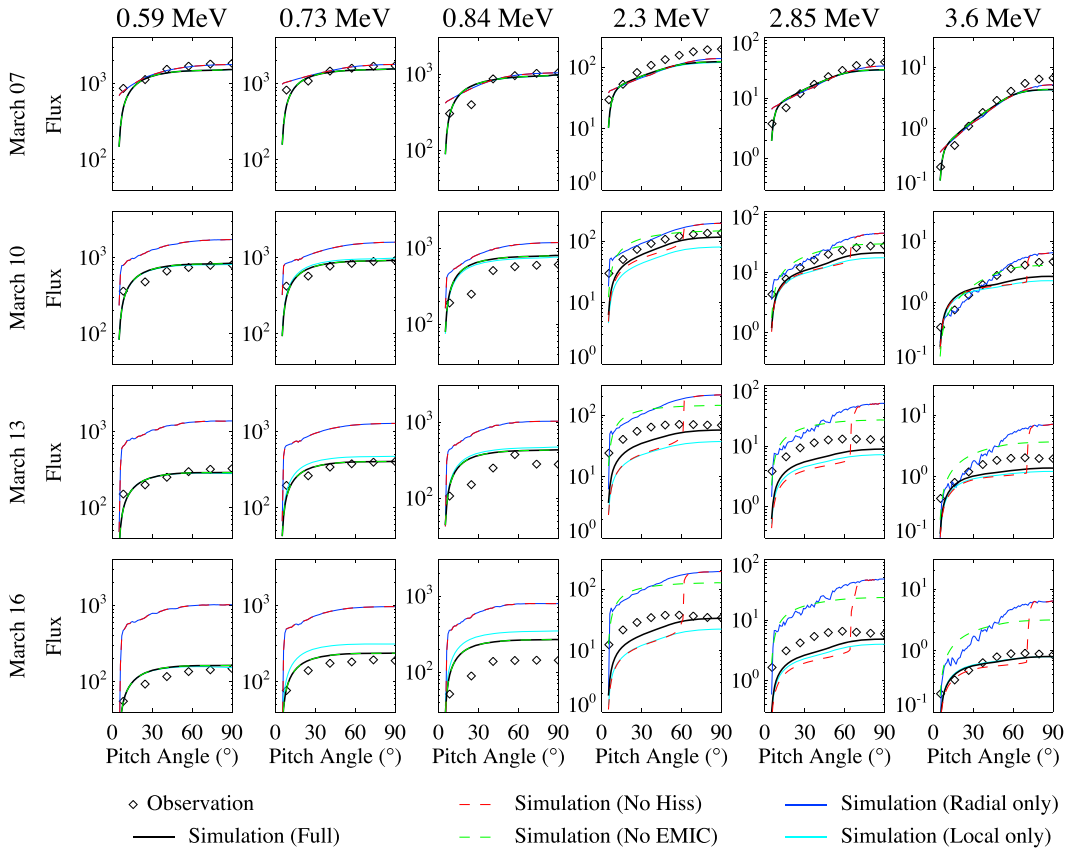

Figure 4. The pitch angle distributions of electron fluxes at $L = 4.5$ for energies of 0.59–3.60 MeV at 00:00 UT on 7–16 March 2013. The black diamonds indicate the observed electron flux values, and various lines represent the simulation results from the full simulation (black solid line), simulation without hiss wave scattering (red dashed line), simulation without EMIC wave scattering (green dashed line), pure radial diffusion simulation (blue solid line), and pure local diffusion simulation (cyan solid line), respectively. At energies below ~1 MeV, the full simulation profile nearly overlaps with the profile of simulation without EMIC waves, and the profile of radial diffusion nearly overlaps with the profile of simulation without hiss waves, because EMIC waves cannot scatter the low-energy electrons ($<$ ~1 MeV).

scattering processes lead to the formation of the observed flattened pitch angle distribution profiles from 0.59 to 3.6 MeV. The ongoing cross calibration work on the MagEIS data will slightly increase the observed flux levels in the highest MagEIS energy channels (~1–2 MeV), which would have little effects on our general comparison results above. It is interesting to note that there exists a minimum at ~90° pitch angle over 0.84–2.85 MeV from the observed electron pitch angle distribution (diamond symbols in Figure 4), but the cause of this feature is not clear at this stage.

4. Conclusions and Discussions

The gradual diffusion of energetic electrons in March 2013 is an ideal event to study quiet time radial diffusion and pitch angle scattering processes in the Earth's outer radiation belt. The MagEIS and REPT instruments on board the Van Allen Probes provide high-resolution particle data in both time and energy near the equatorial plane in the radiation belts. Following the injections after the geomagnetic storm on 1 March, the electrons gradually diffused inward by ~0.5 R_E and slowly decayed by approximately an order of magnitude from 6 to 16 March, until the arrival of a strong interplanetary shock on 17 March.

We used a three-dimensional radiation belt model to simulate the evolution of energetic electron fluxes during the 10 day quiet period. The radial diffusion process in our simulation produces L time profiles of energetic electrons consistent with the observations. The global plasmaspheric hiss model constructed based on in situ wave measurements by Van Allen Probes and THEMIS, together with a statistical hiss wave distribution, provides reasonable loss rates for the electrons below ~1 MeV, and including pitch angle

scattering by weak EMIC wave activity based on the statistical results is able to account for the loss of the electrons above ~1 MeV. The pitch angle scattering by hiss waves also caused the observed flattened pitch angle distributions over a wide range of pitch angles. The coupled processes of radial diffusion and pitch angle scattering by the plasmaspheric hiss and EMIC waves successfully reproduced the essential features of electron dynamics during the 10 day quiet period in March 2013. It is important to note that the EMIC wave model used in our study is based on statistical results and may not represent the actual wave evolution during this 10 day period. Nevertheless, we demonstrate that an additional loss mechanism is needed to scatter MeV electrons more efficiently than that by plasmaspheric hiss alone and show that pitch angle scattering by weak EMIC waves is able to account for >MeV electron loss, consistent with the observation. Recently, *Kersten et al.* [2014] have also found that the EMIC wave scattering can be a significant loss process for the high-energy electrons with energies greater than ~2 MeV using time-averaged EMIC wave power over long periods, which agrees with our conclusions about the roles of EMIC waves.

During quiet periods, the gradual diffusion behavior of energetic electrons is a common feature observed by the Van Allen Probes [*Baker et al.*, 2013, 2014]. Since the radial diffusion and pitch angle scattering by weak to modest plasma waves are persistent over long periods, similar electron evolution features may be explained by the diffusion processes described here. Our study suggests that the coupled radial diffusion and pitch angle scattering processes are important in the long-term evolution of energetic electrons in the Earth's radiation belts.

Acknowledgments

This work was supported by NASA grant NNX11AR64G and by JHU/APL contracts 967399 and 921647 under NASA's prime contract NAS5-01072 and NSF grants AGS 1405041 and 1405054. The analysis at UCLA was supported by the EMFISIS subaward 1001057397:01 and by the ECT subaward 13–041. B. Ni acknowledges the support from the NSFC grants 41204120 and 41474141 and from the Fundamental Research Funds for the Central Universities grant 2042014kf0251. We acknowledge the Van Allen Probe data from the EMFISIS instrument obtained from http://emfisis.physics.uiowa.edu/data/index/, data from the MagEIS and REPT instruments obtained from http://www.rbsp-ect.lanl.gov/data_pub/, and the THEMIS data obtained from http://themis.ssl.berkeley.edu/data/themis/ under NAS5-02099. We thank the World Data Center for Geomagnetism, Kyoto, for providing the *Kp* indices (http://wdc.kugi.kyoto-u.ac.jp/kp/index.html) and the Space Physics Data Facility at the NASA Goddard Space Flight Center for providing the OMNI2 data (ftp://spdf.gsfc.nasa.gov/pub/data/omni/omni_cdaweb/).

The Editor thanks three anonymous reviewers for their assistance in evaluating this paper.

References

Agapitov, O., A. Artemyev, V. Krasnoselskikh, Y. V. Khotyaintsev, D. Mourenas, H. Breuillard, M. Balikhin, and G. Rolland (2013), Statistics of whistler-mode waves in the outer radiation belt: Cluster STAFF-SA measurements, *J. Geophys. Res. Space Physics*, *118*, 3407–3420, doi:10.1002/jgra.50312.

Albert, J. M., and S. L. Young (2005), Multidimensional quasi-linear diffusion of radiation belt electrons, *Geophys. Res. Lett.*, *32*, L14110, doi:10.1029/2005GL023191.

Angelopoulos, V. (2008), The THEMIS mission, *Space Sci. Rev.*, *141*, 5–34, doi:10.1007/s11214-008-9336-1.

Baker, D. N., et al. (2012), The Relativistic Electron Proton Telescope (REPT) instrument on board the Radiation Belt Storm Probes (RBSP) spacecraft: Characterization of Earth's radiation belt high-energy particle populations, *Space Sci. Rev.*, doi:10.1007/s11214-012-9950-9.

Baker, D. N., et al. (2013), A long-lived relativistic electron storage ring embedded in Earth's outer Van Allen belt, *Science*, *340*(6129), 186–190, doi:10.1126/science.1233518.

Baker, D. N., et al. (2014), Gradual diffusion and punctuated phase space density enhancements of highly relativistic electrons: Van Allen Probes observations, *Geophys. Res. Lett.*, *41*, 1351–1358, doi:10.1002/2013GL058942.

Blake, J. B., et al. (2013), The Magnetic Electron Ion Spectrometer (MagEIS) instruments aboard the Radiation Belt Storm Probe (RBSP) spacecraft, *Space Sci. Rev.*, doi:10.1007/s11214-013-9991-8.

Brautigam, D. H., and J. M. Albert (2000), Radial diffusion analysis of outer radiation belt electrons during the October 9, 1990 magnetic storm, *J. Geophys. Res.*, *105*(A1), 291–309, doi:10.1029/1999JA900344.

Cornwall, J. M. (1972), Radial diffusion of ionized helium and protons: A probe for magnetospheric dynamics, *J. Geophys. Res.*, *77*(10), 1756–1770, doi:10.1029/JA077i010p01756.

Glauert, S. A., and R. B. Horne (2005), Calculation of pitch angle and energy diffusion coefficients with the PADIE code, *J. Geophys. Res.*, *110*, A04206, doi:10.1029/2004JA010851.

Horne, R. B., and R. M. Thorne (1998), Potential waves for relativistic electron scattering and stochastic acceleration during magnetic storms, *Geophys. Res. Lett.*, *25*(15), 3011–3014, doi:10.1029/98GL01002.

Kennel, C. F., and F. Engelmann (1966), Velocity space diffusion from weak plasma turbulence in a magnetic field, *Phys. Fluids*, *9*, 2377–2388, doi:10.1063/1.1761629.

Kersten, T., R. B. Horne, S. A. Glauert, N. P. Meredith, B. J. Fraser, and R. S. Grew (2014), Electron losses from the radiation belts caused by EMIC waves, *J. Geophys. Res. Space Physics*, *119*, 8820–8837, doi:10.1002/2014JA020366.

Kletzing, C. A., et al. (2013), The Electric and Magnetic Field Instrument Suit and Integrated Science (EMFISIS) on RBSP, *Space Sci. Rev.*, doi:10.1007/s11214-013-9993-6.

Lee, J. H., and V. Angelopoulos (2014), On the presence and properties of cold ions near Earth's equatorial magnetosphere, *J. Geophys. Res. Space Physics*, *119*, 1749–1770, doi:10.1002/2013JA019305.

Li, W., Y. Y. Shprits, and R. M. Thorne (2007), Dynamic evolution of energetic outer zone electrons due to wave-particle interactions during storms, *J. Geophys. Res.*, *112*, A10220, doi:10.1029/2007JA012368.

Li, W., et al. (2014), Radiation belt electron acceleration by chorus waves during the 17 March 2013 storm, *J. Geophys. Res. Space Physics*, *119*, 4681–4693, doi:10.1002/2014JA019945.

Lyons, L. R. (1974a), General relations for resonant particle diffusion in pitch angle and energy, *J. Plasma Physics*, *12*, 45–49, doi:10.1017/S0022377800024910.

Lyons, L. R. (1974b), Pitch angle and energy diffusion coefficients from resonant interactions with ion cyclotron and whistler waves, *J. Plasma Physics*, *12*, 417–432, doi:10.1017/S002237780002537X.

Lyons, L. R., and R. M. Thorne (1973), Equilibrium structure of radiation belt electrons, *J. Geophys. Res.*, *78*(13), 2142–2149, doi:10.1029/JA078i013p02142.

Mauk, B. H., N. J. Fox, S. G. Kanekal, R. L. Kessel, D. G. Sibeck, and A. Ukhorskiy (2012), Science objectives and rationale for the Radiation Belt Storm Probes mission, *Space Sci. Rev.*, *179*(1–4), 3–27, doi:10.1007/s11214-012-9908-y.

Meredith, N. P., R. M. Thorne, R. B. Horne, D. Summers, B. J. Fraser, and R. R. Anderson (2003), Statistical analysis of relativistic electron energies for cyclotron resonance with EMIC waves observed on CRRES, *J. Geophys. Res.*, *108*(A6), 1250, doi:10.1029/2002JA009700.

Meredith, N. P., R. B. Horne, R. M. Thorne, D. Summers, and R. R. Anderson (2004), Substorm dependence of plasmaspheric hiss, *J. Geophys. Res.*, *109*, A06209, doi:10.1029/2004JA010387.

Meredith, N. P., R. B. Horne, J. Bortnik, R. M. Thorne, L. Chen, W. Li, and A. Sicard-Piet (2013), Global statistical evidence for chorus as the embryonic source for plasmaspheric hiss, *Geophys. Res. Lett.*, *40*, 2891–2896, doi:10.1002/grl.50593.

Meredith, N. P., R. B. Horne, T. Kersten, B. J. Fraser, and R. S. Grew (2014), Global morphology and spectral properties of EMIC waves derived from CRRES observations, *J. Geophys. Res. Space Physics*, *119*, 5328–5342, doi:10.1002/2014JA020064.

Ni, B., R. M. Thorne, Y. Y. Shprits, and J. Bortnik (2008), Resonant scattering of plasma sheet electrons by whistler-mode chorus: Contribution to diffuse auroral precipitation, *Geophys. Res. Lett.*, *35*, L11106, doi:10.1029/2008GL034032.

Ni, B., R. M. Thorne, N. P. Meredith, R. B. Horne, and Y. Y. Shprits (2011), Resonant scattering of plasma sheet electrons leading to diffuse auroral precipitation: 2. Evaluation for whistler mode chorus waves, *J. Geophys. Res.*, *116*, A04219, doi:10.1029/2010JA016233.

Ni, B., J. Bortnik, R. M. Thorne, Q. Ma, and L. Chen (2013), Resonant scattering and resultant pitch angle evolution of relativistic electrons by plasmaspheric hiss, *J. Geophys. Res. Space Physics*, *118*, 7740–7751, doi:10.1002/2013JA019260.

Ni, B., et al. (2014), Resonant scattering of energetic electrons by unusual low-frequency hiss, *Geophys. Res. Lett.*, *41*, 1854–1861, doi:10.1002/2014GL059389.

Ozeke, L. G., I. R. Mann, K. R. Murphy, I. Jonathan Rae, and D. K. Milling (2014), Analytic expressions for ULF wave radiation belt radial diffusion coefficients, *J. Geophys. Res. Space Physics*, *119*, 1587–1605, doi:10.1002/2013JA019204.

Reeves, G. D., K. L. McAdams, R. H. W. Friedel, and T. P. O'Brien (2003), Acceleration and loss of relativistic electrons during geomagnetic storms, *Geophys. Res. Lett.*, *30*(10), 1529, doi:10.1029/2002GL016513.

Ripoll, J.-F., J. M. Albert, and G. S. Cunningham (2014), Electron lifetimes from narrowband wave-particle interactions within the plasmasphere, *J. Geophys. Res. Space Physics*, *119*, 8858–8880, doi:10.1002/2014JA020217.

Roux, A., O. Le Contel, C. Coillot, A. Bouabdellah, B. de la Porte, D. Alison, S. Ruocco, and M. C. Vassal (2008), The search coil magnetometer for THEMIS, *Space Sci. Rev.*, *141*, 265–275, doi:10.1007/s11214-008-9371-y.

Sakaguchi, K., Y. Kasahara, M. Shoji, Y. Omura, Y. Miyoshi, T. Nagatsuma, A. Kumamoto, and A. Matsuoka (2013), Akebono observations of EMIC waves in the slot region of the radiation belts, *Geophys. Res. Lett.*, *40*, 5587–5591, doi:10.1002/2013GL058258.

Schulz, M., and L. J. Lanzerotti (1974), *Particle Diffusion in the Radiation Belts*, Springer, New York.

Sheeley, B. W., M. B. Moldwin, H. K. Rassoul, and R. R. Anderson (2001), An empirical plasmasphere and trough density model: CRRES observations, *J. Geophys. Res.*, *106*(A11), 25,631–25,641, doi:10.1029/2000JA000286.

Shprits, Y. Y., and B. Ni (2009), Dependence of the quasi-linear scattering rates on the wave normal distribution of chorus waves, *J. Geophys. Res.*, *114*, A11205, doi:10.1029/2009JA014223.

Shprits, Y. Y., S. R. Elkington, N. P. Meredith, and D. A. Subbotin (2008a), Review of modeling of losses and sources of relativistic electrons in the outer radiation belts: I. Radial transport, *J. Atmos. Sol. Terr. Phys.*, *70*(14), 1679–1693, doi:10.1016/j.jastp.2008.06.008.

Shprits, Y. Y., D. A. Subbotin, N. P. Meredith, and S. R. Elkington (2008b), Review of modeling of losses and sources of relativistic electrons in the outer radiation belts: II. Local acceleration and loss, *J. Atmos. Sol. Terr. Phys.*, *70*(14), 1694–1713, doi:10.1016/j.jastp.2008.06.014.

Spence, H. E., et al. (2013), Science goals and overview of the Energetic Particle, Composition, and Thermal Plasma (ECT) suite on NASA's Radiation Belt Storm Probes (RBSP) mission, *Space Sci. Rev.*, doi:10.1007/s11214-013-0007-5.

Thorne, R. M. (2010), Radiation belt dynamics: The importance of wave-particle interactions, *Geophys. Res. Lett.*, *37*, L22107, doi:10.1029/2010GL044990.

Thorne, R. M., et al. (2013), Evolution and slow decay of an unusual narrow ring of relativistic electrons near L~3.2 following the September 2012 magnetic storm, *Geophys. Res. Lett.*, *40*, 3507–3511, doi:10.1002/grl.50627.

Tsyganenko, N. A., and M. I. Sitnov (2005), Modeling the dynamics of the inner magnetosphere during strong geomagnetic storms, *J. Geophys. Res.*, *110*, A03208, doi:10.1029/2004JA010798.

Turner, D. L., et al. (2014), Competing source and loss mechanisms due to wave-particle interactions in Earth's outer radiation belt during the 30 September to 3 October 2012 geomagnetic storm, *J. Geophys. Res. Space Physics*, *119*, 1960–1979, doi:10.1002/2014JA019770.

Usanova, M. E., et al. (2014), Effect of EMIC waves on relativistic and ultrarelativistic electron populations: Ground-based and Van Allen Probes observations, *Geophys. Res. Lett.*, *41*, 1375–1381, doi:10.1002/2013GL059024.

Xiao, F., Z. Su, H. Zheng, and S. Wang (2009), Modeling of outer radiation belt electrons by multidimensional diffusion process, *J. Geophys. Res.*, *114*, A03201, doi:10.1029/2008JA013580.

Xiao, F., Z. Su, H. Zheng, and S. Wang (2010), Three-dimensional simulations of outer radiation belt electron dynamics including cross-diffusion terms, *J. Geophys. Res.*, *115*, A05216, doi:10.1029/2009JA014541.